SEMARAK ILMU PUBLISHING

Journal of Advanced Research in Fluid Mechanics and Thermal Sciences

Journal homepage:
https://semarakilmu.com.my/journals/index.php/fluid_mechanics_thermal_sciences/index
ISSN: 2289-7879

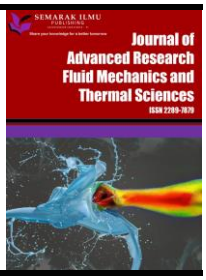

Parameterization of a Refined Model Aimed at Simulating Laser-Induced Incandescence of Soot Using a Visible Excitation Wavelength of 532 nm

Sébastien Menanteau[1], Romain Lemaire[2,*]

[1] Energy, Environment & Materials Engineering, Icam Lille, 59016, France
[2] Department of Mechanical Engineering, École de Technologie Supérieure, Montreal, Quebec, H3C 1K3, Canada

ARTICLE INFO

Article history:
Received 16 March 2022
Received in revised form 20 June 2022
Accepted 29 June 2022
Available online 26 July 2022

Keywords:
Soot; laser-induced incandescence; absorption function; modeling

ABSTRACT

Laser-induced incandescence (LII) is one of the most powerful techniques for soot detection in combustion media. It is therefore commonly used to perform experiments in lab-scale flames and industrial combustors with a view to elucidating the formation mechanisms leading to combustion-generated fine carbonaceous particles while assessing their intrinsic properties. Quantitatively interpreting LII measurements, however, requires a firm knowledge of the optical properties of soot, including their wavelength-dependent absorption function ($E(m,\lambda)$). Among the approaches used to evaluate such a crucial parameter, one can implement a LII model to derive the $E(m,\lambda)$ value which has to be set to reproduce a series of LII signals measured in a well-characterized environment. In this context, the present work aims at parameterizing a refined LII model built upon a comprehensive version of soot heat- and mass-balance equations for $E(m,\lambda)$ assessment when using a visible excitation wavelength of 532 nm. The proposed model integrates terms representing the saturation of linear, single- and multi-photon absorption processes, cooling by sublimation, conduction, radiation and thermionic emission, in addition to mechanisms depicting soot oxidation and annealing, non-thermal photodesorption of carbon clusters, as well as corrective factors accounting for the shielding effect and multiple scattering (MS) within aggregates. To parameterize this advanced simulation tool, an optimization procedure coupling design of experiments with a genetic algorithm-based solver was implemented. Doing so allowed to estimate the values of different factors involved in absorption and sublimation terms, including the multi-photon absorption cross-section for C_2 photodesorption, the saturation coefficients for linear- and multi-photon absorption, as well as the $E(m,532)$ value. Obtained parameters turned out to be well-suited to reproduce a set of LII signals acquired in a Diesel flame. While leading to predictions merging on a single curve with measured data, the so-parameterized model notably led to infer $E(m,532)$ values of 0.30 and 0.38 when considering or neglecting MS within aggregates, respectively. Finally, the $E(m,532)/E(m,1064)$ ratio estimated based on data collected herein and in a former modeling work was found to be consistent with results issued from two-excitation wavelength LII measurements previously reported in the literature.

* *Corresponding author.*
E-mail address: romain.lemaire@etsmtl.ca

https://doi.org/10.37934/arfmts.98.1.92103

1. Introduction

Soot particles emitted by combustion processes have harmful impacts on the environment [1] and human health [2]. Meeting increasingly stringent regulations aimed at restricting particle emissions, however, demands gaining a thorough understanding of the physical-chemical mechanisms underlying their formation, growth and oxidation [3-6]. Doing so is particularly essential for the development and improvement of the computational codes used to design and optimize the performances of combustion devices, including engines [7,8].

During the last decades, continuous efforts have been devoted to the development of advanced in-situ measurement techniques allowing to probe soot particles in complex reacting media in order to elucidate the phenomena at play during their formation [5,6]. Within this context, laser-induced incandescence (LII) has proven to be one of the most powerful diagnostics for soot detection and characterization [9,10]. It consists in heating soot up to its incandescence temperature using a high-energy pulsed-laser source before collecting the quasi-blackbody radiation emitted above the flame emission by means of a photomultiplier tube or a gated intensified camera. Since the magnitude of the prompt LII signals has been demonstrated to be proportional to the soot volume fraction for detection wavelengths comprised in the visible spectral range [11], this technique has been widely implemented to infer information on spatial and temporal distributions of soot in combustion media (see [9,10] and references therein). Based on the fact that the decay rate of the LII signals is a function of the particle-specific surface area, LII has also been used extensively to assess the morphological properties of soot by combining time-resolved detection approaches with LII signal modeling (e.g., [12,13]).

Correctly interpreting laser-based optical measurements, however, requires a firm knowledge of the absorption function of soot $E(m,\lambda)$, whose value significantly differs from one study to another. For instance, $E(m,532)$ values ranging from 0.179 to 0.40 were considered in [14], while [9] proposed an average $E(m,\lambda)$ of 0.3 ± 0.06 for a wavelength range going from the visible to the near-infrared (IR) based on an extensive set of data derived from light extinction measurements [15-20]. Despite such discrepancies, there is consensus regarding the fact that the $E(m,\lambda)$ value of mature soot is likely to be comprised between 0.2 and 0.4 in the visible spectrum, with an uncertainty of about a factor of 2. On the other hand, many works still point out that this parameter is strongly dependent upon the particle maturation stage [21,22] and wavelength [23,24], thus prompting the need for more data on the matter.

Among the strategies implemented to assess the absorption function of soot, one can use a LII model allowing to infer, by inverse calculations, the $E(m,\lambda)$ value which has to be set such as to reproduce a series of LII signals measured in a well-characterized environment [25-28]. In that case, however, a reliable LII model is a must. This especially explains why continued efforts have been made since the early work by [11] to develop calculation tools capable of predicting laser-induced incandescence signals of soot under widely varying operating conditions [10]. Overall, current LII models from the literature, even while differing from one another as a function of the nature of the energy fluxes they consider and of the related governing equations, typically predict radiation from heated soot by introducing the temporal evolution of the soot temperature (T_p) and diameter (D_p) in a Planck function. To that end, the values of T_p and D_p are calculated by solving a couple of differential equations depicting the particle energy and mass balances during the laser heating and subsequent cooling stages. While most of the models are built upon relatively basic heat and mass balance equations, which represent heating by absorption of the laser energy and cooling by heat conduction, radiation and sublimation (see [9,10,14] and references therein), more comprehensive formulations incorporating photolytic processes have still been proposed during the last two

decades. For instance, [14,29] proposed integrating mechanisms which account for soot melting, annealing and oxidation, thermionic emissions, non-thermal photodesorption of carbon clusters from the particle surface and multi-photon absorption leading to the photodesorption of C_2 clusters at high fluences. Using such a type of refined model, [21] predicted theoretical signals matching those measured in co-flow diffusion flames of ethylene. In a subsequent modeling work based on the use of inverse techniques, [30] demonstrated that integrating photolytic mechanisms such as those proposed in [14,29] (e.g., multi-photon absorption and carbon cluster photodesorption) was required to reproduce LII signals over a wide range of fluences. Furthermore, the results from [30] also led to the conclusion that an in-depth analysis of the formulation and parameterization of the sub-models proposed in [14,29] was necessary since, in their current form, those expressions turned out to be unsuitable to reproduce the experimental data measured by [31] in a diffusion flame of ethylene. In an attempt to simulate signals collected in an atmospheric $CH_4/O_2/N_2$ premixed flat flame, [26,32] also performed advanced calculations which confirmed the relevance of considering photolytic mechanisms (e.g., photodesorption of carbon clusters) while providing interesting insights into the importance of soot annealing to properly model LII at high fluences.

Based on the conclusions drawn from the above literature survey, we recently proposed and parameterized one of the most refined LII models ever, with the aim of simulating an extensive set of signals measured in a Diesel flame using a 1064-nm excitation wavelength [27,28]. To this end, we implemented a comprehensive version of the soot heat- and mass-balance equations, including terms which account for saturation of linear, single- and multi-photon absorption, cooling by sublimation, conduction, radiation and thermionic emission, in addition to mechanisms depicting soot oxidation and annealing, non-thermal photodesorption of carbon clusters, as well as corrective factors accounting for the shielding effect and multiple scattering (MS) within soot aggregates. In an original fashion, an optimization procedure coupling a design of experiments with a genetic algorithm-based solver was introduced in order to parameterize the so-proposed model formulation. As such, predicted signals merging on a single curve with measured ones were obtained at different heights above the burner in the low-to-intermediate fluence regime [28]. While allowing to assess soot properties and empirical factors whose values were quite rare (if not inexistent) for a 1064-nm laser excitation wavelength (e.g., multi-photon absorption cross-section and saturation coefficients for linear- and multi-photon absorption), the modeling tool developed in [27,28] also turned out to be well-suited to simulate the evolution of the peak LII signals as a function of the laser fluence measured in different combustion environments, including premixed and diffusion flames of gaseous and liquid fuels [26,27,31]. The present paper, which is a continuation of this broader research dealing with LII modeling, covers the simulation of signals collected in the Diesel flame previously studied in [27,28], but using a laser source operating at 532 nm. In this context, the parameterization procedure proposed in [27,28] has been used to infer the values of key factors seldom reported in the literature, including the multi-photon absorption cross-section for C_2 photodesorption, the empirical saturation coefficients for linear and multi-photon absorption, as well as the enthalpy required to photodesorb carbon clusters, in addition to the soot absorption function. While demonstrating the predictive capability of the proposed model through comparisons between measured and simulated signals, the present work also assesses some factors (e.g., aggregate size and wavelength) prone to influence the absorption function of soot.

2. Methodology

2.1 Experiment

The experimental setup used in the present work is similar to the one implemented in [27,28]. It will thus only be briefly described in the following.

For the flame generation system, it is based on Lemaire's spray burner configuration, which was used in [24,33-35] and characterized in [36]. It consists of a McKenna hybrid flat flame burner composed of a 60-mm diameter porous bronze plate on which a lean premixed methane-air flat flame is stabilized. A direct injection high efficiency nebulizer introduced into a central 6.35-mm diameter tube allows atomizing the low-sulfur diesel fuel which immediately ignites when crossing the hot gases produced by the flat flame. By setting flow rates identical to those used in [27,28], one obtains a turbulent diffusion flame around 18 cm in height and 2 cm wide. Due to the presence of polycyclic aromatic hydrocarbons (PAHs) at low heights above the burner (HAB), LII measurements were carried out at 110 mm HAB to avoid any interference with signals originating from PAHs, which can fluoresce upon visible excitation [37] at lower HAB in this flame [38].

The LII setup, which is described in [27], is composed of a Continuum Nd:YAG laser operating at 1064 nm, equipped with a frequency doubling crystal to generate the first harmonic at 532 nm. The central part of the Gaussian laser beam was selected using a 1-mm diaphragm to obtain a beam section of 0.0021 cm^2 at $1/e^2$ at the center of the burner, as monitored using a Gentec CCD beam profiler. LII signals were collected perpendicularly to the laser propagation direction using a 300-µm horizontal slit placed in front of a Hamamatsu R2257 photomultiplier tube. An OG-550 long pass filter and two 532-nm cutoff filters were, moreover, used to reduce the measurement noise caused by the flame emission as well as to reject radiation at 532 nm. Signals were finally digitized and stored by means of a Teledyne Lecroy oscilloscope. Additional information regarding the measurement procedure can be found in [24].

2.2 LII Model

Like with any LII model from the literature, the radiation from laser-heated soot was simulated by introducing the temporal evolution of the soot temperature (T_p) and diameter (D_p) in a Planck function. To this end, variations of T_p and D_p were calculated by solving a couple of differential equations depicting the variations of the internal energy rate ($\frac{dU_{int}}{dt}$) and mass ($\frac{dM_p}{dt}$) of the particles composing soot aggregates as a function of time. As in [28], the mechanisms considered to build the refined model used in the present work include terms representing particle heating by absorption of the laser energy ($\dot{Q}_{abs}$), soot annealing ($\dot{Q}_{ann}$), oxidation ($\dot{Q}_{ox}$) and cooling by radiation ($\dot{Q}_{rad}$), thermionic emission ($\dot{Q}_{th}$), sublimation ($\dot{Q}_{sub}$) and conduction ($\dot{Q}_{cond}$)

$$\begin{cases} \frac{dU_{int}}{dt} = \dot{Q}_{abs} + \dot{Q}_{ann} + \dot{Q}_{ox} - \dot{Q}_{rad} - \dot{Q}_{th} - \dot{Q}_{sub} - \dot{Q}_{cond} \\ \frac{dM_p}{dt} = \sum_{j=1}^{5} \left(\frac{dM_p}{dt}\right)_{sub,j} + \left(\frac{dM_p}{dt}\right)_{ox} \end{cases} \quad (1)$$

where subscripts 'sub' and 'ox' denote the contributions of the sublimation and oxidation mechanisms to the mass loss, respectively, while 'j' stands for the contribution of each vaporized carbon cluster C_j to the particle mass loss. As far as the rate of change of the internal energy is concerned, it was formulated as detailed in [29] to differentiate between the contributions of the unannealed (subscript 's') and annealed (subscript 'a') soot fractions (noted X in Eq. (2)), such that:

$$\frac{dU_{int}}{dt} = N_p \cdot \frac{\pi}{6} \cdot {D_p}^3 \cdot \frac{d\,T_p}{dt} \cdot [\rho_s \cdot c_s \cdot X_s + \rho_a \cdot c_a \cdot X_a] \tag{2}$$

in which N_p is the number of primary particles in an aggregate, while ρ and c stand for the density and specific heat, respectively. Regarding D_p, it was expressed as a function of M_p as per Eq. (3).

$$D_p = \left[\frac{6 \cdot M_p}{\pi} \cdot \left(\frac{X_s}{\rho_s} + \frac{X_a}{\rho_a}\right)\right]^{1/3} \tag{3}$$

The absorption flux, for its part, was expressed based on the formulation provided in [14] to account for saturation of the linear, single- and multi-photon absorption processes. It was, moreover, adapted as in [27,28] to take into account the contributions of both unannealed and annealed soot fractions following an equation of the type

$$\dot{Q}_{abs} = \dot{Q}_{abs,s} + \dot{Q}_{abs,a} \tag{4}$$

with

$$\dot{Q}_{abs,r} = C_{abs,r}^{multi}(\lambda, N_p) \cdot \frac{f_{1,r} \cdot B_{\lambda 1,r}}{\int_0^{t_l} q_{exp}(t)dt} \cdot \left\{1 - exp\left[-\frac{F \cdot q_{exp}(t)}{B_{\lambda 1,r}}\right]\right\} + N_p \cdot \frac{n \cdot h \cdot c_l}{\lambda_l} \cdot k_{\lambda n,r} \tag{5}$$

where the subscript 'r' represents either 's' or 'a', while $f_{1,r}$ and $B_{\lambda 1,r}$ are empirical factors related to the single-photon absorption process, q_{exp} is the normalized laser irradiance, t_l and F represent the laser pulse duration and fluence, respectively, n is the number of photons to be adsorbed to photodesorb C_2 clusters, h stands for the Planck constant, c_l is the speed of light and λ_l corresponds to the laser excitation wavelength. As for $C_{abs,r}^{multi}$, it denotes the soot absorption cross-section whose expression integrates the corrective factor from [39], which allows to account for the internal multiple scattering (MS) within soot aggregates [40] when N_p>1 (the classical Rayleigh-Debye-Gans theory for Fractal Aggregates (RDG-FA) applying otherwise)

$$C_{abs,r}^{multi}(\lambda, N_p) = N_{tot} \cdot C_{abs,r}^{mono} \cdot h_{\lambda,N_p} \cdot N_p \cdot p(N_p) \tag{6}$$

As for the terms in Eq. (6), N_{tot} represents the aggregate number density, $C_{abs,r}^{mono}$ corresponds to the absorption cross-section of a primary particle (with $C_{abs,s}^{mono} = X_s \cdot \frac{\pi^2 \cdot {D_p}^3}{\lambda_l} \cdot E(m,\lambda)$ and $C_{abs,a}^{mono} = X_a \cdot \frac{\pi^2 \cdot {D_p}^3}{\lambda_l} \cdot f_a \cdot E_a(m,\lambda)$), $p(N_p)$ stands for the probability density function of the aggregate size, and h_{λ,N_p} corresponds to the MS corrective factor proposed in [39]. Regarding the term $k_{\lambda n,r}$ which is present in Eq. (5), it depicts the rate constant for the removal of C_2 clusters by photodesorption, and is calculated using the following equation

$$k_{\lambda n,r} = X_r \cdot \frac{\lambda_l}{n \cdot h \cdot c_l} \cdot \frac{\sigma_{\lambda n,r} \cdot \pi \cdot {D_p}^3 \cdot N_{sr}}{6} \cdot \frac{(B_{\lambda n,r})^n}{\int_0^{t\infty} [q_{exp}(t)]^n dt} \cdot \left\{1 - exp\left[-\left(\frac{F \cdot q_{exp}(t)}{B_{\lambda n,r}}\right)^n\right]\right\} \tag{7}$$

where X_r is equal to either X_s or X_a, $\sigma_{\lambda n,r}$ represents the multi-photon absorption cross-section for the photodesorption of C_2 clusters, N_{sr} is the density of carbon atoms on the surface of primary

particles (2.8×10^{15} cm^{-2} for unannealed and 3.8×10^{15} cm^{-2} for annealed soot [29]), while $B_{\lambda n,r}$ is an empirical saturation coefficient for multi-photon absorption.

As far as annealing ($\dot{Q}_{ann}$) and oxidation ($\dot{Q}_{ox}$) fluxes are concerned, they were expressed based on the formulations proposed in [29] and [41], respectively, in which N_p was introduced. Similarly, N_p was embedded within the governing equations representing the radiation and thermionic emission fluxes, which were equated as proposed in [29] and [14], respectively (see [28] for more details regarding the expression of $\dot{Q}_{ann}$, $\dot{Q}_{ox}$, $\dot{Q}_{rad}$ and $\dot{Q}_{th}$). It should finally be noted that although the formulation proposed by [42] to represent the energy loss induced by the thermal ejection of electrons from heated particles was identified as being more adapted than the one issued from [14], the latter was still considered in this preliminary analysis for comparison purposes with the results obtained when using the model parameters listed in [14].

Regarding the sublimation sub-model, it was derived from the one extensively presented in [29] (see Eq. (8)), although the rate constants for the photodesorption of C_2 clusters for both unannealed and annealed soot fractions were adapted from [14] to compute the effective pressures $P_{\lambda s}$ and $P_{\lambda a}$:

$$\dot{Q}_{sub} = -N_p \cdot \sum_{j=1}^{5} \frac{1}{W_j} \cdot \left(\frac{dM_p}{dt}\right)_{sub,j} \cdot \left[\frac{\Delta H_j \cdot \left(P_{sat}^{C_j} - P_{\lambda s} - P_{diss} - P_{\lambda a}\right) + \Delta H_{\lambda n,s} \cdot P_{\lambda s} + \Delta H_{diss} \cdot P_{diss} + \Delta H_{\lambda n,a} \cdot P_{\lambda a}}{P_{sat}^{C_j}}\right] \quad (8)$$

with W_j being the molecular weight of the C_j species, ΔH_j the enthalpy of formation of the carbon vapor species C_j, $\Delta H_{\lambda n,s}$ and $\Delta H_{\lambda n,a}$ the enthalpy required to photodesorb C_j clusters from unannealed and annealed particles, respectively, $P_{sat}^{C_j}$ the saturation partial pressure and P_{diss} the effective pressure issued from the rate of thermal photodesorption from the annealed soot fraction [28].

To conclude, a Fuchs equivalent sphere modeling approach integrating the shielding corrective factor from [43] was selected to compute the conductive cooling rate. Doing so allows to calculate the conduction rates in the free-molecular (FM) and continuum (C) regimes based on the following equations

$$\dot{Q}_{cond,FM} = \frac{1}{8} \cdot \pi \cdot \alpha_T \cdot {D_{HC}}^2 \cdot P_g \cdot \sqrt{\frac{8 \cdot k_B \cdot T_\delta}{\pi \cdot M_g}} \cdot \frac{\gamma^* + 1}{\gamma^* - 1} \cdot \left(\frac{T_p}{T_\delta} - 1\right) \quad (9)$$

$$\dot{Q}_{cond,C} = 4 \cdot \pi \cdot \left(\frac{D_{HC}}{2} + \delta\right) \cdot \int_{T_g}^{T_\delta} k_g(T) dT \quad (10)$$

where α_T stands for the thermal accommodation coefficient (equal to 0.47 for N_p=139 [28]), P_g represents the ambient pressure, k_B corresponds to the Boltzmann constant, M_g is the average mass of the gas molecules, γ^* denotes the mean value of the heat capacity ratio, δ and T_δ are the distance and temperature related to the limiting sphere separating the free-molecular from the continuum regime, T_p and T_g correspond to the particle and surrounding gas temperatures, k_g stands for the heat conduction coefficient of the surrounding gas, while D_{HC} represents the equivalent sphere diameter related to the shielding corrective factor defined in [43].

Calculations were performed using the soot properties (i.e., D_p=20 nm and N_p=139) and the gas temperature (i.e., T_g=1704 K) previously reported in [28]. By solving the coupled differential equations summarized in Eq. (1), one can infer the variations of T_p and D_p as a function of space and

time, whose values can then be introduced into a Planck function integrated over the spectral range of the detection system as detailed in [28]. To that end, the spatial distribution of the laser energy was numerically reproduced and discretized using 17 × 17 elements. The simulated LII signals were finally calculated over the entire laser beam dimensions before being integrated over the spatial domain corresponding to the 300-µm slit used during experiments for proper comparisons with measured data.

3. Results and Discussion

The values of the parameters integrated within the governing equations accounting for the energy fluxes composing the differential equations depicted in Eq. (1) were set as explained in section 2.2 and in the reference [28]. A few variables, whose values are barely available in the literature, however, needed to be estimated, including the multi-photon absorption cross-section for C_2 photodesorption ($\sigma_{\lambda n,s}$), the empirical saturation coefficients for linear ($B_{\lambda 1,s}$) and multi-photon ($B_{\lambda n,s}$) absorption, the enthalpy required to photodesorb carbon clusters ($\Delta H_{\lambda n,s}$) and the soot absorption function $E(m,532)$. Although such parameters were assessed for a 1064-nm laser wavelength in [28], their values have never been reported for soot irradiated with a 532-nm excitation source, except in [14], where the following values were proposed: $E(m,532)$=0.34, $B_{\lambda 1,s}$=0.6 J·cm^{-2}, $B_{\lambda n,s}$=0.5 J·cm^{-2}, $\sigma_{\lambda n,s}$=1.9×10^{-10} cm^{2n-1}·J^{1-n} and $\Delta H_{\lambda n,s}$=3.4×10^{5} J·mol^{-1} (see table 1).

Table 1
Parameters for $\dot{Q}_{abs}$ and $\dot{Q}_{sub}$

Parameter	[14]	Present study
$E(m,\lambda)$	0.34 (without MS)	0.30 (with MS) 0.38 (without MS)
$\sigma_{\lambda n,s}$ (cm^{2n-1}·J^{1-n})	1.9×10^{-10}	7.6×10^{-10}
$B_{\lambda 1,s}$ (J·cm^{-2})	0.6	0.58
$B_{\lambda n,s}$ (J·cm^{-2})	0.5	0.35
$\Delta H_{\lambda n,s}$ (J·mol^{-1})	3.4×10^{5}	3.4×10^{5}

Although the model used in [14] diverges from the one implemented herein, the above parameters were still tested as a first step. As shown in Figure 1, their integration within the model used in the present work, however, turned out to be unsuitable to properly reproduce the LII fluence curve and time decays measured at 110 mm HAB in the Diesel flame. An underprediction of the peak LII signals is indeed systematically observed in the 0.03-0.18 J·cm^{-2} fluence range (see Figure 1(a)), which quite logically leads to theoretical signal time decays below measured ones (see Figure 1(b)). Consequently, and following the methodology recently introduced in [27,28], a full central composite design of experiments (DoE) was coupled to a genetic algorithm-based optimizer (the ga function of MATLAB®) to identify a set of parameters allowing to obtain simulated signals matching measured ones. To that end, a DoE was first built to find suitable $E(m,532)$ and $\sigma_{\lambda n,s}$ values by defining an objective function based on the minimization of the least square sum between numerical and experimental fluence curves for fluences below the sublimation threshold (other unknown parameters not considered at this stage as they have no impact on the increasing section of the fluence curves, as discussed in [28]).

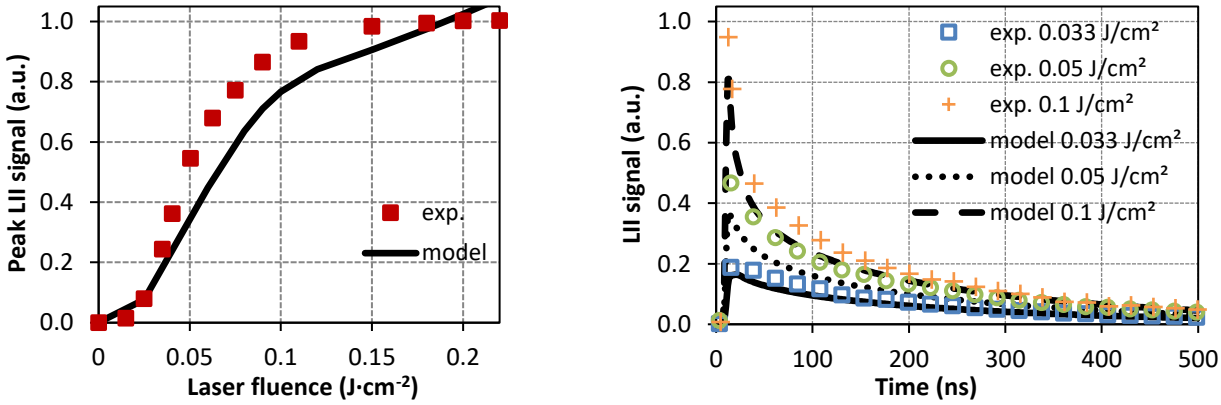

Fig. 1. Comparison of measured (a) LII fluence curves and (b) time decays with predictions issued from the refined model integrating the parameters from [14]

As can be seen by looking at the results reported in Figure 2, this procedure led to the finding of optimized $E(m,532)$ and $\sigma_{\lambda n,s}$ of ~0.31 and ~8.6×10^{-10} cm^{2n-1}·J^{1-n}, noting that the significance and validity of the model were concluded based on an analysis of the variance leading to the obtention of a corresponding Fisher-test p-value less than 10^{-4}, as well as adjusted- and predicted-R^2 values of ~99.8% and ~98.9%, respectively.

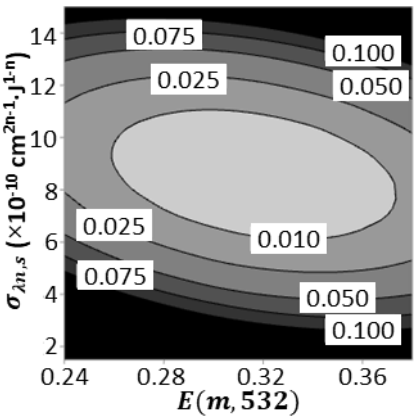

Fig. 2. DoE response surface for $\sigma_{\lambda n,s}$ and $E(m,532)$

The parameterization procedure was then completed by running the genetic algorithm while defining a minimization function based on a least square sum between experimental and numerical LII time decays obtained at each investigated fluence. Intervals of ±15% around the optimum values defined by the DoE were set for $E(m,532)$ and $\sigma_{\lambda n,s}$. For the other parameters, preliminary results issued from a DoE based on the above objective function (i.e., minimization of the least square sum between numerical and experimental LII time decays) led to the identification of the following constraints: 0.2 J·cm^{-2} < $B_{\lambda 1,s}$ < 0.8 J·cm^{-2}, 0.2 J·cm^{-2} < $B_{\lambda n,s}$ < 0.8 J·cm^{-2} and 1.7×10^5 J·mol^{-1} < $\Delta H_{\lambda n,s}$ < 5×10^5 J·mol^{-1}. By considering a population of 20 individuals, it was found that around 150 generations were sufficient to reach the tolerance constraint set to 10^{-4} as in [27]. In doing so, we obtained the following optimized parameters, which are also reported in table 1: $E(m,532)$=0.30, $\sigma_{\lambda n,s}$=7.6×10^{-10} cm^{2n-1}·J^{1-n}, $B_{\lambda 1,s}$=0.58 J·cm^{-2}, $B_{\lambda n,s}$=0.35 J·cm^{-2} and $\Delta H_{\lambda n,s}$=3.4×10^5 J·mol^{-1}. As can be seen by looking at Figure 3, which depicts the LII signals simulated using the above set of parameters, modeled fluence curve and time decays properly reproduce their experimental counterparts.

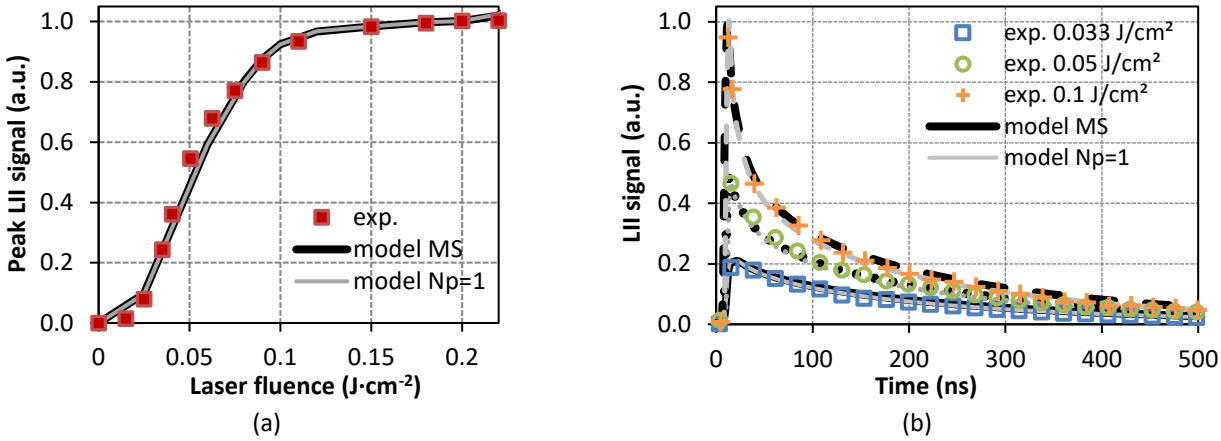

(a) (b)

Fig. 3. Comparison of measured and simulated (a) LII fluence curves and (b) time decays

A similar trend can, moreover, be obtained when neglecting MS (i.e., for N_p=1) provided that an $E(m,532)$ value of 0.38 is set (α_T being considered equal to 0.32 for its part according to [27]). The 21% drop of the soot absorption function estimated when considering the effect of multiple scattering is consistent with the trend that could have been expected based on the data reported in [28], while clearly highlighting the importance of thoroughly considering aggregate properties, to be able to derive consistent information on soot optical properties by LII modeling. It is further of interest to note that the $E(m,532)$ value inferred in this work agrees well with the classical range of values reported in the literature (i.e., between ~0.2 and ~0.4 as mentioned in the introduction).

Looking further at the parameters listed in Table 1, it can be noted that the $\Delta H_{\lambda n,s}$ value found in the present modeling study is identical to that proposed in [14]. Alternatively, the inferred $E(m,532)$, $B_{\lambda n,s}$ and $\sigma_{\lambda n,s}$ values diverge more or less significantly from those reported in [14]. This can be attributed to the sub-models in which multi-photon absorption operates, whose formulations (see section 2.2) diverge from those originally proposed in [14]. Besides, it is of interest to note that the $B_{\lambda 1,s}$ and $B_{\lambda n,s}$ values listed in Table 1 are lower than those estimated in [28] for a 1064-nm excitation wavelength. This is actually well in line with the trends reported in [44], as well as with the fact that the threshold above which the LII response tends to show a lack of fluence dependence is reached for lower F values at 532 nm (close to ~0.1 J·cm^{-2} against ~0.2 J·cm^{-2} at 1064 nm [28]). This is, moreover, consistent with the fact that the shorter the wavelength, the higher the absorption cross-section [10], which is confirmed by the $C_{abs,s}^{multi}$ assessed herein and in [28] for wavelengths of 532 and 1064 nm, respectively. Finally, it is noteworthy that the $E(m,532)$ values found whether neglecting (i.e., N_p = 1) or considering MS (i.e., N_p = 139) are identical to those estimated in [28] when performing LII measurements at the same location within the same flame, but using a 1064-nm excitation wavelength. This therefore leads to estimate $E(m,532)/E(m,1064)$ ratios equal to 1 in both cases (i.e., with or without considering MS), thus indicating a relative lack of wavelength-dependence of the soot absorption function in the visible to IR range, in accordance with previous results obtained when implementing the so-called two-excitation wavelength LII technique [24,39,45].

4. Conclusion

The present work covered the parameterization of a refined model aimed at simulating LII signals collected in a Diesel spray flame using an excitation wavelength of 532 nm. By implementing an advanced optimization procedure coupling design of experiments with a genetic algorithm-based

solver, the values of different factors involved in absorption and sublimation sub-models were assessed, including the multi-photon absorption cross-section for C_2 photodesorption, the empirical saturation coefficients for linear and multi-photon absorption, the enthalpy required to photodesorb carbon clusters and the soot absorption function. More particularly, the following values were inferred: $\sigma_{\lambda n,s}$=7.6×10^{-10} cm^{2n-1}·J^{1-n}, $B_{\lambda 1,s}$=0.58 J·cm^{-2}, $B_{\lambda n,s}$=0.35 J·cm^{-2}, $\Delta H_{\lambda n,s}$=3.4×10^{5} J·mol^{-1} and $E(m,532)$=0.30. Using these parameters, simulated fluence curves and time decays matching their experimental counterparts were obtained. Besides, the present work also led to an evaluation of an $E(m,532)$ which was 21% higher when neglecting the internal multiple scattering within soot aggregates, thus illustrating the importance of considering aggregate properties to derive proper soot absorption function values by LII. Finally, an $E(m,532)/E(m,1064)$ ratio of 1 was estimated in agreement with the data reported in different LII studies [24,39,45]. This modeling work therefore paves the way towards the extension of the predictive ability of refined LII models to simulate data collected using different excitation wavelengths. Further validation against data measured in different combustion environments as well as complementary studies exploring the modeling of LII signals acquired with UV laser sources are still required, however. These provide interesting avenues for future works to be undertaken.

Acknowledgement
This research was supported by the Natural Sciences and Engineering Research Council of Canada (NSERC) and by the John R. Evans Leaders Fund from the Canada Foundation for Innovation (CFI).

References

[1] Highwood, Eleanor J., and Robert P. Kinnersley. "When smoke gets in our eyes: The multiple impacts of atmospheric black carbon on climate, air quality and health." *Environment International 32* (2006): 560-566. https://doi.org/10.1016/j.envint.2005.12.003

[2] Lippmann, Morton. "Toxicological and epidemiological studies of cardiovascular effects of ambient air fine particulate matter (PM2.5) and its chemical components: coherence and public health implications." *Critical Reviews in Toxicology 44*, no. 4 (2014): 299-347. https://doi.org/10.3109/10408444.2013.861796

[3] Richter, Henning, and Jack B. Howard. "Formation of polycyclic aromatic hydrocarbons and their growth to soot—a review of chemical reaction pathways." *Progress in Energy and Combustion Science* 26 (2000): 565-608. https://doi.org/10.1016/S0360-1285(00)00009-5

[4] McEnally, Charles S., Lisa D. Pfefferle, Burak Atakan, and Katharina Khose-Höinghaus. "Studies of aromatic hydrocarbon formation mechanisms in flames: Progress towards closing the fuel gap." *Progress in Energy and Combustion Science* 32 (2006): 247-294. https://doi.org/10.1016/j.pecs.2005.11.003

[5] Desgroux, Pascale, Xavier Mercier, and Kevin A. Thomson. "Study of the formation of soot and its precursors in flames using optical diagnostics." *Proceedings of the Combustion Institute* 34, no. 1 (2013): 1713-1738. https://doi.org/10.1016/j.proci.2012.09.004

[6] Michelsen, Hope A. "Probing soot formation, chemical and physical evolution, and oxidation: A review of in situ diagnostic techniques and needs." *Proceedings of the Combustion Institute* 36, no. 1 (2017): 717-735. https://doi.org/10.1016/j.proci.2016.08.027

[7] Raj, R. Thundil Karuppa, and R. Manimaran. "Effect of swirl in a constant speed DI diesel engine using computational fluid dynamics." *CFD Letters* 4, no. 4 (2012): 214-224.

[8] Zulkurnai, Fatin Farhanah, Wan Mohd Faizal Wan Mahmood, Norhidayah Mat Taib, and Mohd Radzi Abu Mansor. "Simulation of combustion process of diesel and ethanol fuel in reactivity controlled compression ignition engine." *CFD Letters* 13, no. 2 (2021): 1-11. https://doi.org/10.37934/cfdl.13.2.111

[9] Schulz, Christof, Boris F. Kock, Max Hofmann, Hope A. Michelsen, Stefan Will, Bas Bougie, Rainer Suntz, and Greg J. Smallwood. "Laser-induced incandescence: recent trends and current questions." *Applied Physics B 83*, no 1 (2006): 333-354. https://doi.org/10.1007/s00340-006-2260-8

[10] Michelsen, Hope A., Christof Schulz, Greg J. Smallwood, and Stefan Will. "Laser-induced incandescence: Particulate diagnostics for combustion, atmospheric, and industrial applications." *Progress in Energy and Combustion Science 51*, no. 1 (2015): 2-48. https://doi.org/10.1016/j.pecs.2015.07.001

[11] Melton, Lynn A. "Soot diagnostics based on laser heating." *Applied Optics 23* (1984): 2201–2208. https://doi.org/10.1364/AO.23.002201
[12] Will, Stefan, Stephan Schraml, Katharina Bader, and Alfred Leipertz. "Performance characteristics of soot primary particle size measurements by time-resolved laser-induced incandescence." *Applied Optics 37* (1998): 5647-5658. https://doi.org/10.1364/AO.37.005647
[13] Michelsen, Hope A., Peter O. Witze, David Kayes, and Simone Hochgreb. "Time-resolved laser-induced incandescence of soot: the influence of experimental factors and microphysical mechanisms." *Applied Optics 42* (2003): 5577-5590. https://doi.org/10.1364/AO.42.005577
[14] Michelsen, Hope A., Fengshan Liu, Boris F. Kock, Henrik Bladh, Andrej Boiarciuc, et al. "Modeling laser-induced incandescence of soot: a summary and comparison of LII models." *Applied Physics B 87*, no. 1 *(*2007): 503-521. https://doi.org/10.1007/s00340-007-2619-5
[15] Bruce, Charles W., Thor F. Stromberg, Kristian P. Gurton, and Joel B. Mozer. "Trans-spectral absorption and scattering of electromagnetic radiation by diesel soot." *Applied Optics 30* (1991): 1537-1546. https://doi.org/10.1364/AO.30.001537
[16] Dobbins, Richard A., George W. Mulholland, and Nelson P. Bryner. "Comparison of a fractal smoke optics model with light extinction measurements." *Atmospheric Environment 28* (1994): 889-897. https://doi.org/10.1016/1352-2310(94)90247-X
[17] Choi, Mun-Young, George W. Mulholland, Anthony Hamins, and Takashi Kashiwagi. "Comparisons of the soot volume fraction using gravimetric and light extinction techniques." *Combustion and Flame 102* (1995): 161-169. https://doi.org/10.1016/0010-2180(94)00282-W
[18] Krishnan, Sivakumar S., Kuocheng Lin, and Gerard M. Faeth. "Optical properties in the visible of overfire soot in large buoyant turbulent diffusion flames." *Journal of Heat Transfer 122* (2000): 517-524. https://doi.org/10.1115/1.1288025
[19] Krishnan, Sivakumar S., Kuocheng Lin, and Gerard M. Faeth. "Extinction and scattering properties of soot emitted from buoyant turbulent diffusion flames." *Journal of Heat Transfer 123* (2001): 331-339. https://doi.org/10.1115/1.1350823
[20] Schnaiter, Martin, Helmuth Horvath, Ottmar Möhler, Karl Heinz Naumann, Harald Saathoff, and O.W. Schöck. "UV-VIS-NIR spectral optical properties of soot and soot-containing aerosols." *Aerosol Science 34* (2003): 1421-1444. https://doi.org/10.1016/S0021-8502(03)00361-6
[21] López-Yglesias, Xerxes, Paul E. Schrader, and Hope A. Michelsen. "Soot maturity and absorption cross sections." *Journal of Aerosol Science 75* (2014): 43-64. https://dx.doi.org/10.1016/j.jaerosci.2014.04.011
[22] Olofsson, Nils-Erik, Johan Simonsson, Sandra Török, Henrik Bladh, and Per-Erik Bengtsson. "Evolution of properties for aging soot in premixed flat flames studied by laser-induced incandescence and elastic light scattering." *Applied Physics B 119* (2015): 669-683. https://doi.org/10.1007/s00340-015-6067-3
[23] Köylü, Ümit Özgür. "Quantitative analysis of in situ optical diagnostics for inferring particle/aggregate parameters in flames: implications for soot surface growth and total emissivity." *Combustion and Flame 109* (1997): 488-500. https://doi.org/10.1016/S0010-2180(96)00179-4
[24] Yon, Jérôme, Romain Lemaire, Eric Therssen, Pascale Desgroux, Alexis Coppalle, and Kuan Fang Ren. "Examination of wavelength dependent soot optical properties of diesel and diesel/rapeseed methyl ester mixture by extinction spectra analysis and LII measurements." *Applied Physics B 104*, no. 1 (2011): 253-271. https://doi.org/10.1007/s00340-011-4416-4
[25] Snelling, David R., Fengshan Liu, Greg J. Smallwood, and Ömer L. Gülder. "Determination of the soot absorption function and thermal accommodation coefficient using low-fluence LII in a laminar coflow ethylene diffusion flame." *Combustion and Flame 136*, no. 1 (2004): 180-190. https://doi.org/10.1016/j.combustflame.2003.09.013
[26] Bejaoui, Salma, Sébastien Batut, Eric Therssen, Nathalie Lamoureux, Pascale Desgroux, and Fengshan Liu. "Measurements and modeling of laser-induced incandescence of soot at different heights in a flat premixed flame." *Applied Physics B 118*, no. 1 (2015): 449-469. https://doi.org/10.1007/s00340-015-6014-3
[27] Menanteau, Sébastien, and Romain Lemaire. "Analysis of the influence of the conduction sub-model formulation on the modeling of laser-induced incandescence of diesel soot aggregates." *Entropy 22*, no. 1 (2020): 1-14. https://doi.org/10.3390/e22010021
[28] Lemaire, Romain, and Sébastien Menanteau. "Modeling laser-induced incandescence of Diesel soot - Implementation of an advanced parameterization procedure applied to a refined LII model accounting for shielding effect and multiple scattering within aggregates for α_T and E(m) assessment." *Applied Physics B 127*, no. 138 (2021): 1-19. https://doi.org/10.1007/s00340-021-07665-y
[29] Michelsen, Hope A. "Understanding and predicting the temporal response of laser-induced incandescence from carbonaceous particles." *Journal of Chemical Physics 118*, no. 1 *(*2003): 7012-7045. https://doi.org/10.1063/1.1559483

[30] Lemaire, Romain, and Mohamed Mobtil. "Modeling laser-induced incandescence of soot: a new approach based on the use of inverse techniques." *Applied Physics B 119* (2015): 577-606. https://doi.org/10.1007/s00340-015-6032-1

[31] Goulay, Fabien, Paul E. Schrader, Xerxes López-Yglesias, and Hope A. Michelsen. "A data set for validation of models of laser-induced incandescence from soot: temporal profiles of LII signal and particle temperature." *Applied Physics B 112* (2013): 287-306. https://doi.org/10.1007/s00340-013-5504-4

[32] Menanteau, Sébastien, and Romain Lemaire. "Modeling laser-induced incandescence of soot particles produced in a premixed CH4/O2/N2 flat flame." *Proceedings of the 8th International Conference on Fluid Flow, Heat and Mass Transfer* (2021). https://doi.org/10.11159/ffhmt21.139

[33] Lemaire, Romain, Eric Therssen, and Pascale Desgroux. "Effect of ethanol in gasoline and gasoline-surrogate on soot formation in turbulent spray flames." *Fuel 89* (2010): 3952-3959. https://doi.org/10.1016/j.fuel.2010.06.031

[34] Lemaire, Romain, Salma Bejaoui, and Eric Therssen. "Study of soot formation during the combustion of Diesel, rapeseed methyl ester and their surrogates in turbulent spray flames." *Fuel 107* (2013): 147-161. http://dx.doi.org/10.1016/j.fuel.2012.12.072

[35] Lemaire, Romain, Denis Lapalme, and Patrice Seers. "Analysis of the sooting propensity of C-4 and C-5 oxygenates: Comparaison of sooting indexes issued from laser-based experiments and group additivity approaches." *Combustion and Flame 162* (2015): 3140-3155. http://dx.doi.org/10.1016/j.combustflame.2015.03.018

[36] Lemaire, Romain, Mathieu Maugendre, Thierry Schuller, Eric Therssen, and Jérôme Yon. "Original use of a direct injection high efficiency nebulizer for the standardization of liquid fuels spray flames." *Review of Scientific Instruments 80* (2009):105105. https://doi.org/10.1063/1.3249561

[37] Bejaoui, Salma, Romain Lemaire, and Eric Therssen. "Analysis of laser-induced fluorescence spectra obtained in spray flames of Diesel and rapeseed methyl ester using the multiple-excitation wavelength laser-induced incandescence technique with IR, UV and visible excitations." *Combustion Science and Technology 187* (2015): 906-924. http://dx.doi.org/10.1080/00102202.2014.973949

[38] Lemaire, Romain, Alexandro Faccinetto, Eric Therssen, Michaël Ziskind, Cristian Focsa, and Pascale Desgroux. "Experimental comparison of soot formation in turbulent flames of diesel and surrogate diesel fuels." *Proceedings of the Combustion Institute* 32, no. 1 (2009): 737-744. https://doi.org/10.1016/j.proci.2008.05.019

[39] Yon, Jérôme, Eric Therssen, Fengshan Liu, Salma Bejaoui, and Damien Hebert. "Influence of soot aggregate size and internal multiple scattering on LII signal and the absorption function variation with wavelength determined by the TEW-LII method." *Applied Physics B 119*, no. 1 *(*2015): 643-655. https://doi.org/10.1007/s00340-015-6116-y

[40] Yon, Jérôme, Fengshan Liu, Alexandre Bescond, Chloé Caumont-Prim, Claude Rozé, François-Xavier Ouf, and Alexis Coppalle. "Effects of multiple scattering on radiative properties of soot fractal aggregates." *Journal of Quantitative Spectroscopy & Radiative Transfer 133* (2014): 374-381. http://dx.doi.org/10.1016/j.jqsrt.2013.08.022

[41] Michelsen, Hope A., Mark A. Linne, Boris F. Kock, Markus Hofmann, Ben Tribalet, and Christof Schulz. "Modeling laser-induced incandescence of soot: enthalpy changes during sublimation, conduction, and oxidation." *Applied Physics B 93*, no. 1 (2008): 645-656. https://doi.org/10.1007/s00340-008-3181-5

[42] Mitrani, James M., Mikhail N. Schneider, Brentley C. Stratton, and Yevgeny Raitses. "Modeling thermionic emission from laser-heated nanoparticles." *Applied Physics Letters 108* (2016): 054101. http://dx.doi.org/10.1063/1.4940992

[43] Liu, Fengshan, Melissa Yang, Frances A. Hill, David R. Snelling, and Greg J. Smallwood. "Influence of polydisperse distributions of both primary particle and aggregate size on soot temperature in low-fluence LII." *Applied Physics B 83*, no. 1 (2006): 383-395. https://doi.org/10.1007/s00340-006-2196-z

[44] Michelsen, Hope A., Alexei V. Tivanski, Mary K. Gilles, Laura H. van Poppel, Mark A. Dansson, and Peter R. Buseck. "Particle formation from pulsed laser irradiation of soot aggregates studied with a scanning mobility particle sizer, a transmission electron microscope, and a scanning transmission x-ray microscope." *Applied Optics 46*, no. 6 (2007): 959-977. https://doi.org/10.1364/ao.46.000959

[45] Bejaoui, Salma, Romain Lemaire, Pascale Desgroux, and Eric Therssen. "Experimental study of the E(m,λ)/E(m, 1064) ratio as a function of wavelength, fuel type, height above the burner and temperature." *Applied Physics B 116*, no. 1 (2014): 313-323. https://doi.org/10.1007/s00340-013-5692-y